Bidirectional antimonide laser diodes: application to the development of an infrared probe based on absorption spectroscopy

A. Vicet, Bruno Cousin, M. Jahjah, Yves El Kaïm, Y. Rouillard, B. Jaillard

Bidirectional antimonide laser diodes: application to the development of an infrared probe based on absorption spectroscopy

A. Vicet, B. Cousin, M. Jahjah, Y. El Kaim, Y. Rouillard, and B. Jaillard

Abstract We present a study of a sensor probe based on tunable diode laser absorption spectroscopy, using antimonide-based diode lasers emitting at 2.3 and 2.6 μm. The lasers were fabricated by molecular beam epitaxy in the IES laboratory. The active regions are based on InGaAsSb/AlGaAsSb quantum wells grown on a GaSb(N) substrate. The diode lasers operate at room temperature in a continuous wave (CW) regime and exhibit 5 mW of emitted power.

A linear optical setup using the two emitting facets of the diode lasers was developed. By using a second derivative detection by wavelength modulation spectroscopy, we obtained a CH_4 detection limit of 9 ppm m. The sensor is designed to be used in soil and to measure CH_4, CO_2 and H_2O, which are important constituents of the soil atmosphere generated by anaerobic digestion, microbial respiration or water transfer.

1 Introduction

Semiconductor laser based sensors have been introduced in absorption spectroscopy in the 1970s using lead salt diode lasers. Due to their wavelength tuning characteristics and their narrow emission linewidth, tunable diode laser absorption spectroscopy (TDLAS) detection technique has demonstrated high sensitivity and selectivity in the infrared spectral range. The development of telecommunications (InP) and near-infrared antimonide (GaSb) devices that required no cooling, as well as the invention in the 1990s of quantum cascade lasers led to reliable semiconductor lasers emitting from 1.3 μm to greater than 10 μm. TDLAS has been widely used in environmental, industrial process analysis, biological, and medical applications, as for example CO_2 detection in enological applications [1], NO measurements in exhaled air as a biomarker for asthmatic inflammation [2], and CH_4 flux from rice fields [3].

Diode lasers based on InP are more mature and well adapted to trace gas detection but their emission wavelength below 2 μm only reaches weak overtone and combination bands, which does not make these lasers candidates for high sensitivity measurements. Semiconductor lasers based on the use of low bandgap materials (diode lasers as well as quantum cascade lasers) are efficient and many applications have utilized their emission at longer wavelengths capable of reaching fundamental transitions of target trace gas species.

In this paper we describe the development of a TDLAS sensor probe using antimonide-based diode lasers.

This sensor is designed to be used in soil, in different conditions:

– In soils saturated with water, as rice fields [4], natural mangrove soils [5] or waste-activated sludge during anaerobic digestion [6] where the physical (gas diffusion coefficient) and physico-chemical (redox potential) conditions are favorable to CO_2 accumulation and CH_4 production by microbial activities.

A. Vicet (✉) · M. Jahjah · Y. Rouillard
IES, UMR CNRS 5214, CC067, Université Montpellier 2,
Place Eugène Bataillon, 34095 Montpellier cedex 05, France
e-mail: a.vicet@univ-montp2.fr

B. Cousin · Y. El Kaim
LMGC, UMR CNRS 5508, CC048, Université Montpellier 2,
Place Eugène Bataillon, 34095 Montpellier cedex 05, France

B. Jaillard
INRA, UMR Eco&Sols, 2 place Pierre Viala, 34060 Montpellier, France

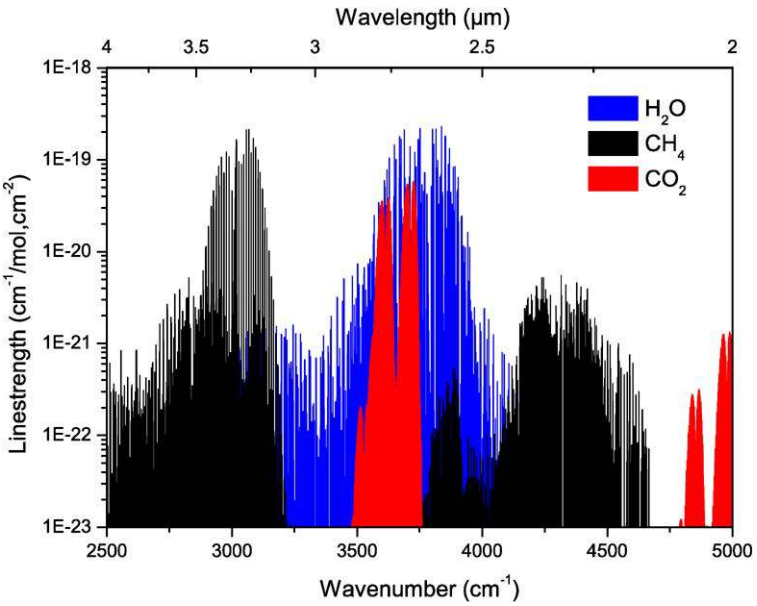

Fig. 1 Absorption line strengths, H_2O, CO_2 and CH_4 between 2 and 4 µm (HITRAN 2004 database [8]). Lasers emitting at 2.3 µm are well adapted to CH_4 detection in an atmospheric transmission window, while lasers at 2.6 µm are suitable for combined H_2O/CH_4 measurements

– In dry soils, therefore well-aerated, the gases of interest are water vapor, and CO_2 which provides an indication of microbial activities.
– In arid soils, for the study of water vapor flux. When water content is low, moisture transfers in soils mainly occurs in the gaseous phase [7]. Continuous measurements of water vapor concentrations at various locations in the soil are therefore important to understand, control and regulate flooding management.

Figure 1 shows the absorption line strengths of water vapor, carbon dioxide and methane from 2 to 4 µm in the infrared range [8]. Due to the spectral line distribution and laser tuning properties (<ten nanometers of continuous tuning), it is not feasible for a sensor to use only one diode laser, to detect simultaneously three target species. With one laser diode it is possible to detect two gases: either H_2O/CO_2 or H_2O/CH_4. It is possible to observe an atmospheric transparency window at 2.3 µm which corresponds to a large methane absorption band with line strengths $>5 \times 10^{-21}$ cm^{-1} mol/cm^{-2}, while at 2.6 µm there is a large water vapor absorption band ($S > 2 \times 10^{-19}$ cm^{-1} mol/cm^{-2}), with a methane line strength of 5×10^{-22} cm^{-1} mol/cm^{-2}. These two wavelengths are therefore suitable either for only CH_4 or simultaneous H_2O and CH_4 detection. Trace gas measurements were performed with the first laser diode at 2.3 µm. A second laser emitting at 2.6 µm is used for CH_4/H_2O detection. First, the characteristics of the antimonide laser diodes developed for the application are described. Then, results of methane detection using a laboratory sensor configured as a soil sensor probe are reported. Then the design of the sensor probe and preliminary tests will also be described.

2 Antimonide laser diodes

The laser devices used in the probe are made from antimonide-based structures grown on *n*-doped GaSb (Te) substrates by solid source molecular beam epitaxy (MBE) in the IES laboratory. The growth of these components is mature and the devices have reached the state of the art in terms of laser performances [9] since the mid 1990s. They have been used in several gas detection systems [10–12]. The lasers work at room temperature, in the continuous wave regime. Detectors adapted to these wavelengths such as InGaAs or InAs photodiodes are efficient, cheap and work at room temperature or with a simple Peltier cooler. The active zone of the devices are constituted of GaInAsSb/AlGaAsSb quantum wells, with compositions and thicknesses dedicated to either 2.3 or 2.6 µm emission.

2.1 A 2.3 µm emission for CH_4 detection without atmospheric interference

The laser structure is constituted of a 75 nm-thick Te-doped *n*-type GaSb buffer, a 90 nm-thick *n*-type layer graded from $Al_{0.10}Ga_{0.90}As_{0.04}Sb_{0.96}$ to $Al_{0.90}Ga_{0.10}As_{0.04}Sb_{0.96}$, a 1 µm-thick *n*-type (2×10^{18} cm^{-3}, Te) $Al_{0.90}Ga_{0.10}As_{0.07}Sb_{0.93}$ cladding layer. These layers were grown at 480°C. The undoped active zone is grown at 420°C and consists of two 16 nm-thick quantum wells made of $Ga_{0.57}In_{0.43}As_{0.13}Sb_{0.87}$ separated by a 30 nm-thick $Al_{0.30}Ga_{0.70}As_{0.03}Sb_{0.97}$ barrier and enclosed between two 375 nm-thick $Al_{0.30}Ga_{0.70}As_{0.07}Sb_{0.93}$ layers constituting the waveguide. Then, a 1 µm-thick *p*-type $Al_{0.90}Ga_{0.10}As_{0.07}Sb_{0.93}$ layer is grown. It is constituted of a 300 nm-thick layer *p*-doped at 5×10^{17} cm^{-3} and a 700 nm-thick layer *p*-doped at

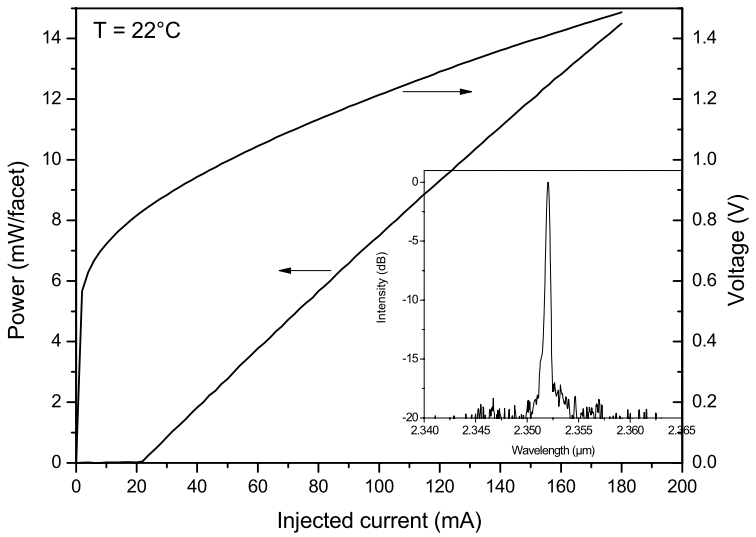

Fig. 2 Light-intensity-voltage curves, for a given laser temperature of 22°C. An emission spectrum is inserted, measured at an injection current of 50 mA at 28°C. The device is a Fabry–Pérot laser, showing a single frequency emission for low injection currents

5×10^{18} cm^{-3}. The growth is ended by a 90 nm-p-type layer graded from $Al_{0.90}Ga_{0.10}As_{0.04}Sb_{0.96}$ to $Al_{0.10}Ga_{0.90}As_{0.04}Sb_{0.96}$ and a 300 nm Be-doped p-type GaSb cap layer.

Thin ridge (5 µm) lasers have then been processed by chemical etching, no facet coating or spectral filtering was added.

The devices are individually mounted episode up on a copper heat-sink. The laser temperature is adjusted with a PID controller (ILX LDT 5910B). The injected current is driven by an ITC 502 laser driver.

The lasers have a low threshold current (22 mA for a 560 µm-long device) with an emitted power reaching more than 16 mW/facet at 160 mA (Fig. 2). The differential quantum efficiency η_d is high, reaching 41%. The exponential increase in threshold current can be fitted with a characteristic temperature $T_0 = 80$ K. The built-in potential is low ($V_D = 0.75$ V) and the serial resistance r_s of 4 Ω shows the good quality of the growth and technological process.

The emission wavelength is centered on 2.36 µm, with a side mode suppression ratio reaching 20 dB under low injection currents. This emission wavelength is adapted to methane detection without atmospheric CO_2 or H_2O interference in ambient air and in soils (low depths) measurements.

The tuning properties of the device have been studied by measuring the transmitted power through a bulk germanium Fabry–Pérot interferometer of 2.34 GHz free spectral range (FSR), leading to a tuning rate of 0.017 nm/mA (or 0.916 GHz/mA).

The CH_4 absorption regions was studied as a function of injected current and laser temperature (absorption map with a reference cell filled with pure CH_4), showing some large absorption lines ($S > 10^{-21}$ cm^{-1} mol/cm^{-2}), which will be suitable to a spectroscopic system.

2.2 A 2.6 µm emission for coupled H_2O/CH_4 detection

To reach an emission wavelength above 2.6 µm, it is necessary to modify the composition of the active zone of the laser diode.

The growth parameters are very similar to those described in the previous paragraph, with the exception of the active zone constituted of two 14 nm-thick $Ga_{0.59}In_{0.41}As_{0.13}Sb_{0.87}$ quantum wells embedded between 28 nm-thick $Al_{0.30}Ga_{0.70}As_{0.03}Sb_{0.97}$ barriers.

A simple ridge technological process has been performed on the wafer, leading to devices showing single frequency emission (typically above the threshold current, up to $2I_{th}$). The emission wavelength is centered on 2.575 µm, with a tuning rate of 2.5 GHz/mA (0.05 nm/mA) (Fig. 3), a value higher than for the 2.3 µm laser described above (due to the higher thermal resistance R_{th} of 100 K W^{-1}). The characteristic temperature of the device is 80 K, with a threshold current value of 21 mA at 20°C for a 700 µm-long device.

The water vapor absorption as a function of temperature and injected current was measured to identify the high-absorption regions (Fig. 4). The absorption lines are obtained by a 3 cm-long path in the ambient air (typically 7750 ppmv of H_2O).

2.3 Bidirectional emission

The use of 2.3/2.6 µm bidirectional laser diodes allows multigas detection, provided that the laser can be tuned over more than one absorption line of different gas species. Figure 5 is an illustration of the kind of measurements that can be performed with a 2.6 µm laser diode, by collecting light from both facets. During the experiment, both channels are used (see details in Sect. 3.1). The first one (channel 1) is a direct open path channel of 5 cm in ambient air. Water

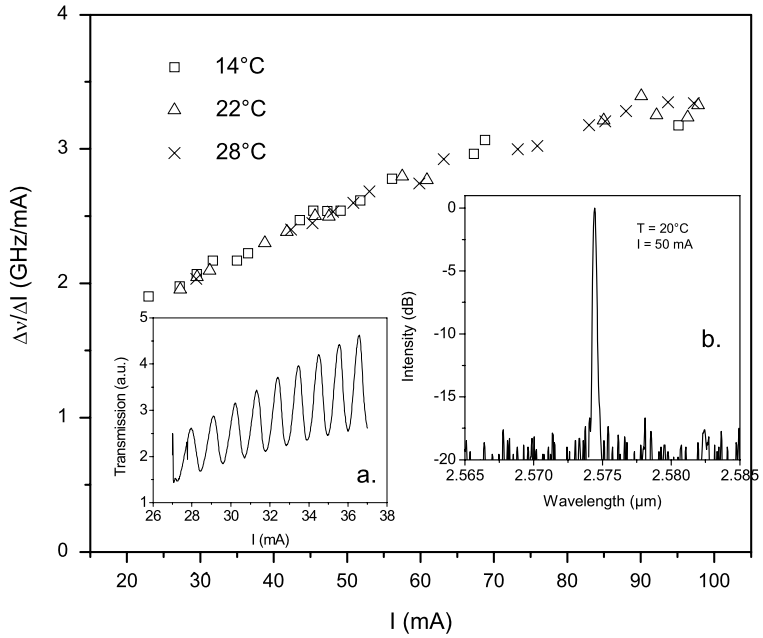

Fig. 3 Tuning properties and emission spectrum of a 2.6 μm Fabry–Pérot laser diode. *Insert* **a**. Fabry–Pérot fringes through a 2.4 GHz FSR Ge FP etalon, current tuning measurement. *Insert* **b**. Emission spectrum, $T = 20°C$, $I = 50$ mA

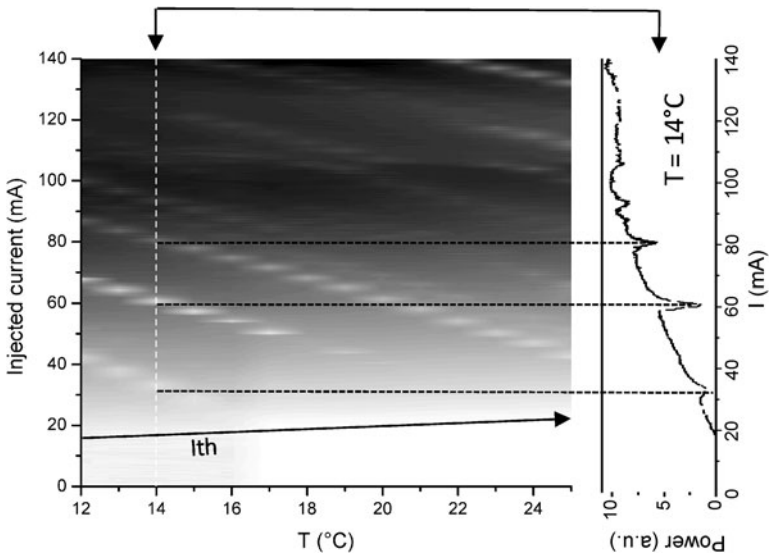

Fig. 4 Water vapor absorption map. A 3 cm-long optical path has been used to scan water absorption lines as a function of injected current and laser temperature. The transmitted optical power is represented *in grey scale*. *The black color* corresponds to the highest power and intense H_2O lines. An example of one of the scans is shown *on the right hand side of the figure*, corresponding to *the dotted line* at 14°C

vapor lines are strong enough to provide a large absorption signature (7750 ppmv). Channel 2 is a longer optical path (20 cm) where a 15 cm-long pure CH_4 cell is inserted in the open path. If the water vapor line can be detected, one can also observe the appearance of methane lines.

3 Methane detection using a laboratory probe sensor

In this section, the results of CH_4 detection tests using a laboratory probe sensor are presented. This probe sensor was not embedded in a tube for an easier access to the sensor components.

3.1 Technical description

Figure 6c represents the optical setup of the laboratory probe sensor. The laser had no facet coatings. As a result, both facets emit identical beams with same power and spectral properties, which was verified with an infrared grating spectrometer and confirmed by gas calibration (Fig. 5). One beam is passed through a reference gas cell while the other beam passes through the measurement cell. Both beams are then detected by means of photodiodes. The beams are collimated with two lenses: a CaF_2 lens, $f = 20$ mm, for the 15 cm-long measurement cell (channel 2) and a Geltech-glass lens, $f = 8$ mm for the 2 cm-long reference cell (channel 1). The beams are then focused on two detectors

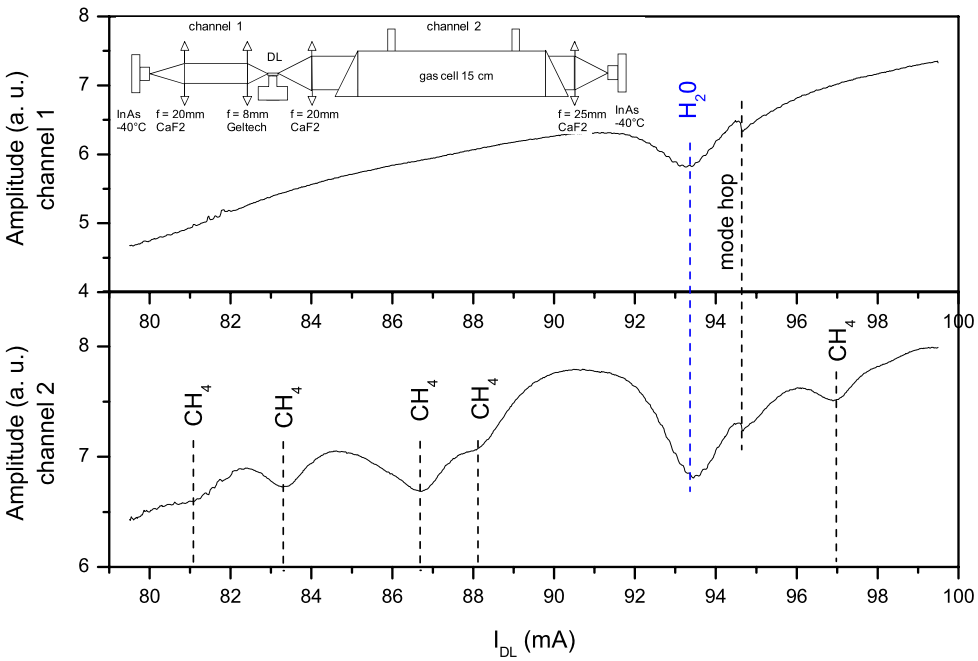

Fig. 5 H_2O and CH_4 simultaneous detection with a 2.6 µm bidirectional laser. A mode hop appears on both channels with a water vapor absorption line (ambient air: 7750 ppmv). On channel 2 (20 cm-long) a 15 cm-long cell filled with pure methane is inserted

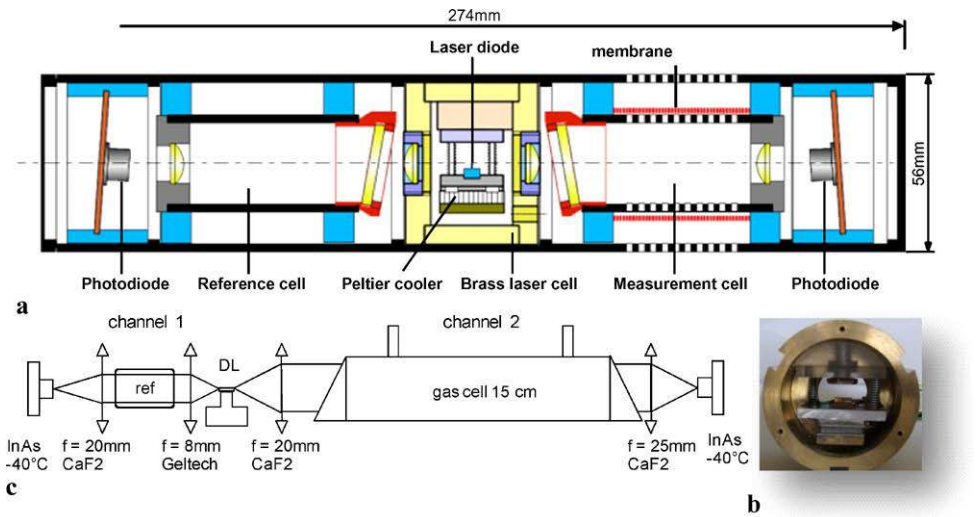

Fig. 6 Sensor probe optical setup: **a** buried probe prototype, **b** brass laser cell, **c** schematic of the prototype (laboratory sensor probe)

with two CaF_2 $f = 20$ mm lenses. As the sensor was developed in the spectral range from 2.3 µm to 4 µm, InAs photodiodes were used as photodetectors. These devices are Peltier-cooled at -40°C and have a detectivity (D^*) of 2×10^{10} cm $\mathrm{Hz}^{1/2}\,\mathrm{W}^{-1}$ at 3 µm. All components (Laser diode and InAs photodiodes) are temperature controlled by a PID (LDT 5910B).

The reference channel is used with a reference cell containing a calibration gas.

3.2 CH_4 detection

The following measurements were performed with a 2.3 µm laser, to calibrate the system without water interference.

We have identified a strong absorption line on which gas measurements have been carried out.

This line is centered at 4249.428 cm^{-1} (2.35341 µm) with a line strength of 2.759×10^{-21} mol $\mathrm{cm}^{-1}/\mathrm{cm}^{-2}$ [8]. Wavelength Modulation Spectroscopy (WMS) was used to perform $2f$ detection. A slow scan (1 Hz) of the injected current (45 to 60 mA) was carried out to scan the absorption line. A high frequency ($f = 9$ kHz) sinusoidal current ($\Delta I = 4.5$ mA $\sim \Delta\nu = 4$ GHz) was superimposed on the laser drive current to modulate the signal. The second harmonic ($2f$) signal amplitude is proportional to the second derivative of the absorption signal [13], since αL value is $\sim 10^{-4}$ for a methane concentration of 1000 ppmv in a 15 cm-long optical path (with α the absorption coefficient of the line in cm^{-1} and L the optical path length in cm).

It was not possible to scan the whole line because a mode hop of the laser appeared at the end of the line. This mode

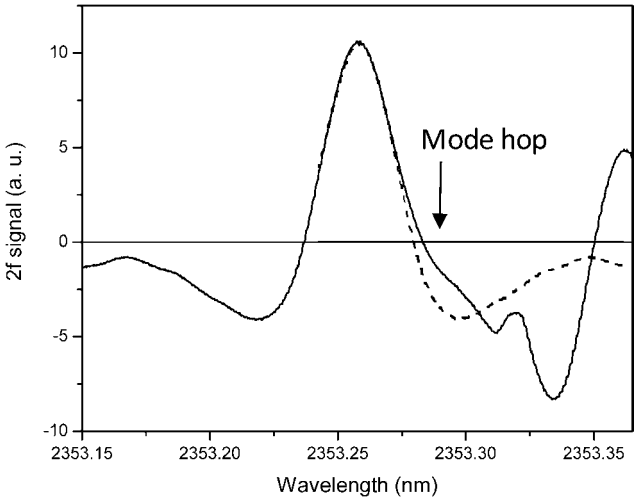

Fig. 7 $2f$ signal, 2.5% CH_4 in a 15 cm-long path. *The arrow* shows the mode hopping zone. *The dotted line* is the ideal $2f$-WMS signal, without mode hop

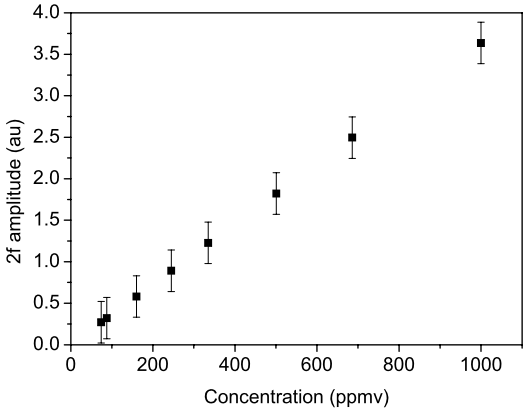

Fig. 8 $2f$-WMS Calibration curve, CH_4 absorption

hop causes a distortion in the absorption line, and thus in the second derivative signal as shown in Fig. 7. The continuous line corresponds to the measured signal: $2f$ detection of 2.5% CH_4 in pure nitrogen at atmospheric pressure, in the 15 cm-long cell at room temperature.

The dotted line corresponds to the ideal $2f$ signal that could be acquired on the right side of the line, without any mode hops. The mode hop can also be observed as a kink on the light-intensity curve (see Fig. 5). This mode hop could not be shifted outside the line without losing single frequency emission. A solution may be working at reduced pressure to narrow the line, but this sensor architecture was limited to atmospheric pressure.

The effect of mode hops is more important at lower concentrations, because the optical noise reaches the signal level. A Fabry–Pérot (FP) fringe interval from 1 to 10 GHz (15 to 2 cm-long optical path in air) can be obtained by reflections on the CaF_2 lenses and on the photodiodes windows, while the absorption linewidth at atmospheric pressure reaches 3 GHz. Under these conditions, care must be taken to make accurate measurements because uncertainties become relatively large compared to the useful signal.

Figure 8 shows a calibration curve acquired by successive gas dilutions in the 15 cm-long absorption cell. The signal amplitude is given by the $2f$ peak value. A detection limit of 60 ppmv (1σ) has been obtained for an absorption path of 15 cm, leading to 9 ppm m absorption limit.

This limit corresponds to $\alpha_{\text{lim}} = 4 \times 10^{-6}$ cm^{-1} and should decrease for a diode laser with a larger single frequency tuning range and by removing the photodiodes windows to avoid the optical noise (FP fringes).

To be applied to soil measurements, the detection limit must be decreased of one or two orders. To reach such a detection limit is not easy with a short optical path length. Two ways may be considered: the use of a small multipass cell with a $2f$-WMS detection scheme (to increase the optical path) or the use of a QEPAS detection scheme. A QEPAS scheme, which could efficiently replace the optical detection following the measurement cell, would be interesting because of its potential increased detection sensitivity with antimonide lasers and the compactness of such a sensor system.

However, the sensor probe will be useful to detect CH_4 leaks in natural mangrove soils [5], lagoons or even leachate collection systems or landfills, were CH_4 emissions can reach concentration levels from 10 to 1000 ppmv [14, 15].

4 Development of the sensor probe

The optical design is similar to the one of the laboratory sensor probe previously described (Fig. 6c) and is based on a linear configuration leading to simple alignment procedures.

In the final (soil buried) configuration, the laser diode will be mounted in a cell made of brass (Fig. 6b), designed to stabilize the laser temperature with efficient thermal dissipation. Its position can be adjusted in three dimensions and the laser beam can be collimated using two CaF_2 ($f = 20$ mm) lenses. The laser cell, the reference gas cell, the measurement cell, the photodiode and the various optical lenses are embedded in a 2 inches diameter aluminum tube. Figure 6a represents the prototype.

The gas contained in the measurement cell must be identical to the gaseous phase of the soil. Consequently, the interface of the measurement cell must allow gaseous transfer while preventing liquid water intrusion. To this end, a hydrophobic membrane is used. An important step of the design of the prototype consisted in verifying that this membrane does not significantly delay the equilibration time between the soil and the measurement cell. A simple test was done to verify this issue.

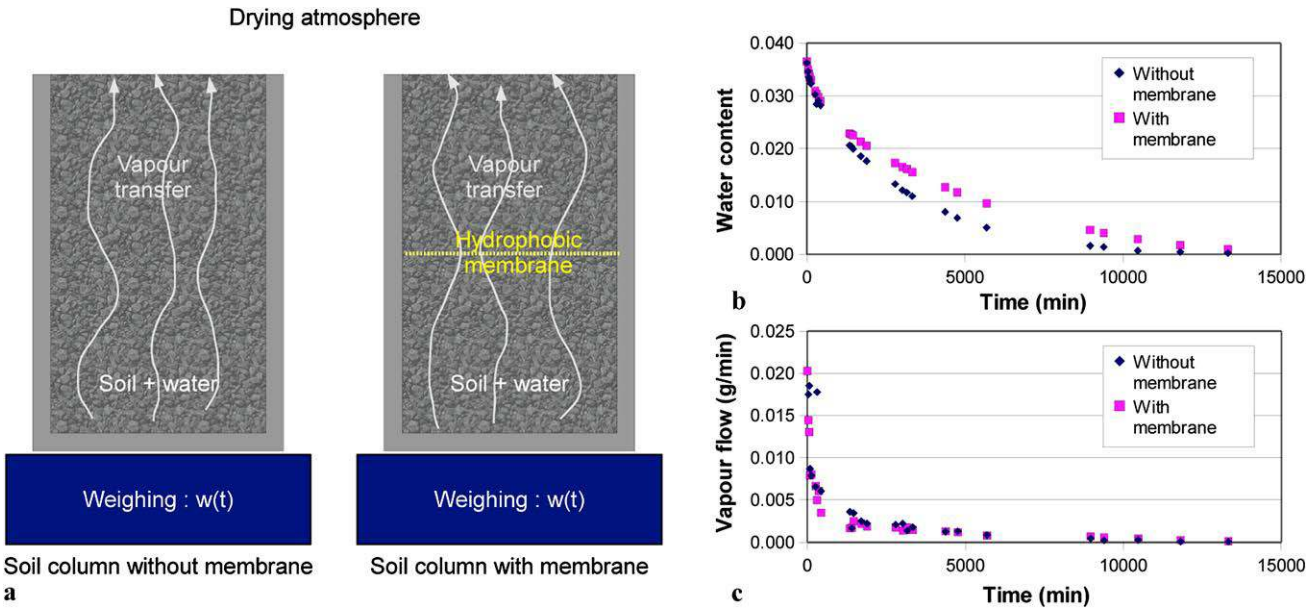

Fig. 9 Test of the hydrophobic membrane, **a** principle of test, **b** drying kinetics, **c** time variation of the vapor flow

Two identical samples of soil were prepared in 60 mm diameter and 100 mm height PVC tubes (Fig. 9a). The initial water content was 3.5% of dry mass of soil. This corresponds to the hygroscopic domain of soil which means that the liquid phase is discontinuous and the mass transfer of water in soil can only occur by vapor transfer. A hydrophobic membrane (Versapor S80277, PALL) was placed at middle height of one of the soil columns and the cylinders were placed in a drying atmosphere. The samples were periodically weighed to determine their water content defined as

$$w = \frac{m_w}{m_d} \tag{1}$$

where m_w is the mass of water in the sample and m_d is the mass of dry soil determined at the end of the experiment after oven drying at 105°C. Figure 9b compares the drying kinetics $w(t)$ of both samples. This figure indicates that the sample which contains the membrane dries more slowly than the other. However, according to our experience, the difference between both kinetics can also be due to variations of the soil characteristics, such as compaction, between the samples. Figure 9c represents the variation of the water flow F_w at the surface of the sample. The water flow is the mass of water vapor leaving the surface of the sample per unit of time. It also corresponds to the mass loss of the sample per unit of time and can be directly deduced from the kinetics:

$$F_w = \frac{dm_w}{dt} = m_d \frac{dw}{dt} \tag{2}$$

Figure 9c shows that the time variation of the water flow is almost the same for both samples. This means that the influence of the membrane is not perceptible in terms of flow of vapor. Even if the kinetics are not identical, their time derivative are similar. Because the flow is associated with the time derivative of the water content, it is more representative of the dynamics of the water vapor transfer.

Considering the characteristic time of the transfer processes in soils which ranges from a few hours to a few weeks, we conclude that the hydrophobic membrane will not significantly alter the equilibration time of the measurement cell.

The next step of our study will test the sensor prototype in soils for various conditions.

5 Conclusions

We have reported the first developments of a laser based probe using a bidirectional optical path but with a simple optical design. Using 2.3 or 2.6 µm antimonide Fabry–Pérot laser diodes, we performed CH_4 detection with a 9 ppm m detection limit, limited by optical noise. The feasibility of a multigas detection was explored with a 2.6 µm diode, allowing for multispecies detection.

The results to date show that the sensor probe is suitable for methane leak measurements in composts, waste-activated sludges, landfills or mangroves (soils with strong microbial activity).

Further, soil measurements are planned with an improved buried sensor probe.

Acknowledgements This work was supported by the STIC and MIPS research departments from Montpellier University and CNRS.

References

1. M. Mulier, V. Zeninari, L. Joly, T. Decarpenterie, B. Parvitte, P. Jeandet, G. Liger-Belair, Appl. Phys. B **94**, 725 (2009)
2. S.M. Cristescu, S.T. Persijn, S.T.E. Lintel Hekkert, F.J.M. Harren, Appl. Phys. B **92**, 343 (2008)
3. P. Werle, K. Maurer, R. Kormann, R. Mucke, F. D'Amato, T. Lancia, A. Popov, Spectrochim. Acta Part A **58**, 2361 (2002)
4. K.H. Tseng, J.L. Tsai, A. Alagesan, B.J. Tsuang, M.H. Yao, P.H. Kuo, Agric. For. Meteorol. **150**, 852 (2010)
5. G.C. Chen, N.F.Y. Tam, Y. Ye, Sci. Total Environ. **408**, 2761 (2010)
6. L. Appels, J. Baeyens, J. Degrève, R. Dewil, Prog. Energy Combust. Sci. **34**, 755 (2008)
7. A. Chammari, B. Naon, F. Cherblanc, J.-C. Bénet, C. R., Méc. **331**, 759 (2003)
8. L.S. Rothman, D. Jacquemart, A. Barbe, D.C. Benner, M. Birk, L.R. Brown, M.R. Carleer, C. Chackerian, K. Chance, L.H. Coudert, V. Dana, V.M. Devi, J.-M. Flaud, R.R. Gamache, A. Goldman, J.M. Hartmann, K.W. Jucks, A.G. Maki, J.-Y. Mandin, S.T. Massie, J. Orphal, A. Perrin, C.P. Rinsland, M.A.H. Smith, J. Tennyson, R.N. Tolchenov, R.A. Toth, J. Vander Auwera, P. Varanasi, G. Wagner, J. Quant. Spectrosc. Radiat. Transf. **96**, 2 (2005)
9. D. Barat, J. Angellier, A. Vicet, Y. Rouillard, L. Le Gratiet, S. Guilet, A. Martinez, A. Ramdane, Appl. Phys. B **90**, 201 (2008)
10. A. Vicet, D.A. Yarekha, A. Perona, Y. Rouillard, S. Gaillard, A.N. Baranov, Spectrochim. Acta A **58**, 2405 (2002)
11. V. Zeninari, A. Vicet, B. Parvitte, L. Joly, G. Durry, Infrared Phys. Technol. **45**, 229 (2004)
12. S. Schilt, A. Vicet, R. Werner, M. Mattiello, L. Thévenaz, A. Salhi, Y. Rouillard, J. Koeth, Spectrochim. Acta A **60**, 3431 (2004)
13. J. Reid, D. Labrie, Appl. Phys. B **26**, 203 (1981)
14. A.M. Fredenslund, C. Cheutz, P. Kjeldsen, Waste Manag. **30**, 2146 (2010)
15. J. Bognerl, K. Spokasl, E. Burtonz, R. Sweeney, V. Corona, Chemosphere **31**, 4119 (1995)